Attitude Determination and Control System Design for a 3U CubeSat to Monitor Forward Light Scattering over Earth Horizon

Mehmet Esit[a]*, Kudakweshe Jeje[a], Ratatamanun Subsinchai[a], Rodrigo Cordova[a], Minh Anh Pham[a], Necmi Cihan Orger[a], Victor Schulz[a], Koju Hiraki[a], Mengu Cho[a]

[a] *Kyushu Institute of Technology, 1-1 Sensui-cho, Tobata-ku, Kitakyushu-shi, Fukuoka, Japan 804-8550*
* Corresponding Author, esit.mehmet109@mail.kyutech.jp

Abstract

The design of the attitude determination and control system (ADCS) of CubeSats plays a crucial role in the success of their missions. ADCS design is a challenging task for CubeSats with commercial-off-the-shelf, low-cost, and small-size equipment due to limited resources. In this paper, the proposed ADCS design of the LEOPARD satellite is presented. The LEOPARD is a 3U cubesat developed by the Kyushu Institute of Technology and its main missions are to perform technology demonstration for an on-orbit positioning system and observe the horizon for light-intensity experiment. The light-intensity experiment requires 8 degree attitude control accuracy to realize its mission. The ADCS of LEOPARD is equipped with two three-axis gyroscopes, two three-axis magnetometers, six coarse sun sensors, a three-axis magnetorquer, and a y-axis reaction wheel. The attitude determination part consists of a coarse attitude determination algorithm that is to be used to initialize the attitude information and an extended Kalman filter as a main attitude estimation technique that makes use of all the sensors. As a backup solution, a gyroless extended Kalman filter is designed in case of gyro failure. An estimation algorithm is designed to determine the residual magnetic moment. The attitude control algorithms provide the satellite detumbling using the B-dot control algorithm and target-pointing PD-type control algorithms. The estimated residual magnetic moment is also compensated by the feedforward control approach. The simulations show that the attitude and angular velocity could be estimated in the Sun phase as well as in eclipse using gyroscope measurements in addition to the magnetometer and sun sensor. Nadir pointing and Sun pointing modes can be realized using solely magnetic actuation within the requirements for communication and Sun acquisition. Horizon detection algorithm with Sun pointing is achieved for scientific missions in sunrise and sunset phases by using a reaction wheel in addition to magnetorquers.
Keywords: LEOPARD, CubeSat, attitude estimation, attitude control, horizon monitoring

Nomenclature

$\boldsymbol{\omega}$	: Angular velocity of the satellite
$\boldsymbol{q}$	: Satellite quaternion
$\boldsymbol{q}_e$	: Error quaternion
$\boldsymbol{b}_{gyro}$	: Gyro bias
$\boldsymbol{M}_{MTQ}$	: Magnetorquer control moment
$\boldsymbol{M}_{RMM}$	: Residual magnetic moment
$\boldsymbol{x}$	: Filter state vector
$\boldsymbol{h}$	: Filter measurement vector
k_{Bdot}	: Control gain for Bdot algorithm
k_{att}	: Control gain for attitude
k_{ω}	: Control gain for angular rate
k_d	: Reaction wheel dumping coefficient
$\boldsymbol{B}_b$	: Magnetic field in body frame
$\boldsymbol{S}_b$	: Sun vector in body frame
$\boldsymbol{N}_b$	: Nadir vector
$\bar{\boldsymbol{r}}$	: Normalized position vector
$\bar{\boldsymbol{v}}$	: Normalized velocity vector
$\boldsymbol{T}_d$	: Desired Torque
T_{rw}	: Reaction wheel torque command
H_{rw}	: Reaction wheel angular momentum

Acronyms/Abbreviations

ADCS	: Attitude Determination and Control System
COTS	: Commercial-off-the-shelf
EKF	: Extended Kalman Filter
LEO	: Low Earth Orbit
RMM	: Residual magnetic moment
RW	: Reaction wheel
TAM	: Three-axis magnetometer
ISS	: International Space Station

1. Introduction

Since the early 2000s, space research has undergone a significant transformation by the rise of CubeSats, driven by innovations in miniaturization and cost-effective development and launch processes. These versatile satellites have become the preferred choice for educational institutions and startups. CubeSats not only serve as excellent platforms for showcasing cutting-edge technologies and offering hands-on training but also excel in conducting valuable scientific missions. Their affordability and educational opportunities have empowered non-spacefaring nations to launch their first satellites, nurturing a new wave of space professionals and fuelling innovation in the field [1].

The success of CubeSat missions relies significantly on the discreet design of their ADCS. This aspect of the mission poses particular challenges due to budget limitations and the need to work within strict constraints on the satellite's mass, size, and volume. To meet these demands, the ADCS for CubeSats typically involves the use of COTS, cost-effective, and compact equipment, making it a complex yet essential part of mission planning.

This study presents the ADCS algorithms and strategy for the LEOPARD satellite. The LEOPARD (Light Intensity Experiment with On-orbit Positioning and Satellite Ranging Demonstration) is a 3U CubeSat mainly developed by the Kyushu Institute of Technology, with the support of Nanyang Technological University. It is planned to be launched into the orbit of the ISS as a precursor mission for a potential lunar CubeSat project called Horyu-VI [2], which is envisioned as a 6U CubeSat mission destined for the Moon. Thus, the LEOPARD mission serves as a platform to demonstrate and test several key technologies and subsystems in LEO. The initial selection of subsystems for testing includes a multispectral camera (MSC) payload and an on-board one-way radio ranging signal processing unit (OPERA) [3]. The multispectral camera payload is designed to detect light scattering caused by atmospheric molecules, resulting in Rayleigh scattering when the Sun is positioned below the horizon. Image sequences are planned to have durations ranging from 3 to 4 minutes. Upon reaching the orbital sunset position, the imaging sequence will start once the Sun has dipped below the horizon, as demonstrated in Fig. 1. Conversely, orbital sunrise monitoring will initiate approximately 3-4 minutes before the Sun becomes visible above the horizon.

In the light-intensity experiment, precise attitude control within an 8-degree accuracy range is required. Additionally, the accuracy of attitude estimation holds significant importance as it directly impacts the precision of the analysis results. This task, which involves precise attitude control, is achieved using the magnetic actuators and the RW. The remaining pointing requirements for tasks such as Sun acquisition and communication are less stringent in terms of precision. These tasks can be achieved through either magnetic actuation solely or in conjunction with the RW.

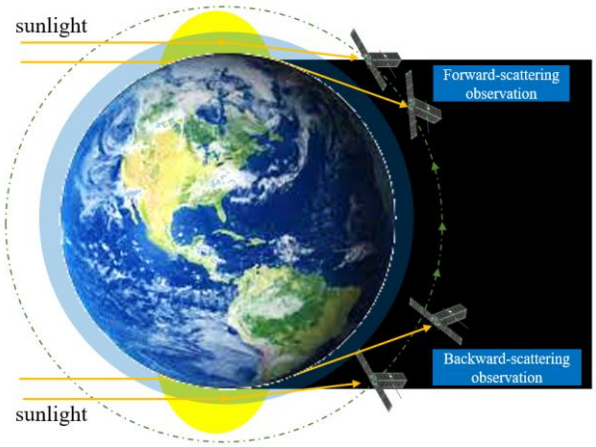

Fig. 1. Sunset and Sunrise horizon monitoring for light-intensity experiment

The paper is structured as follows: Section 2 presents the ADCS design of LEOPARD including ADCS modes, selected equipment, attitude determination methodology, attitude control strategy and methodology. Moving on to Section 3, it presents the simulation environment, simulation results and discussions. Finally, the paper wraps up with a conclusion section.

2. LEOPARD ADCS design

The ADCS structure is illustrated in Fig. 2 using a block diagram. Sensors provide attitude-related information to the attitude estimator block, which fuses measurements to determine attitude and angular rate,

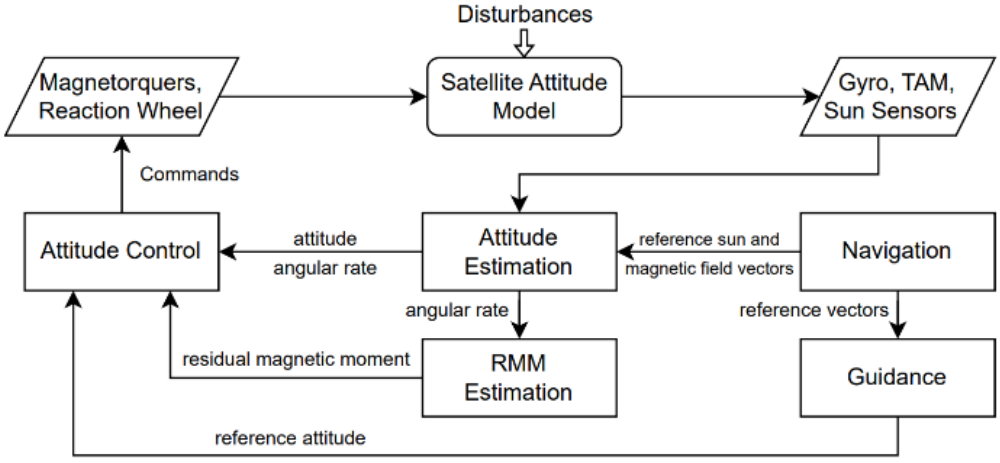

Fig. 2. Block diagram of LEOPARD ADCS

incorporating modeled reference vectors from the navigation block. Additionally, an RMM estimator serves as a second-stage estimator to determine RMM using angular velocity estimates. The RMM estimation is utilized for its feedforward cancellation with magnetorquers in the control block. The control block also calculates feedback control laws using reference and estimated attitude states, and the desired control torque is allocated to the actuators. Lastly, the commanded control actions are applied by the actuators.

Table 1. ADCS Equipment

Qty	Component	Manufacturer	Placement and specifications
6	Sun sensor	Hamamatsu	Si Photodiodes, placed on each side, -40 to +125 °C
1	TAM	PNI Sensor	Placed on -z panel, ±800 µT range, 13 nT sensitivity
2	Gyroscope	STMicroelectronics	3-axis, ±245 dps, 8.75 mdps sensitivity, rate noise spectral density 0.03 dps/√Hz
		TDK InvenSense	3-axis, ±250 dps, 7.63 mdps sensitivity, rate noise spectral density 0.01 dps/√Hz
3	Magnetorquer+TAM	ISIS	0.2 Am^2, two torque rods and one air core torque
1	Reaction wheel	CubeSpace	Placed on y-axis, ±8000 rpm range, 1.77 mNms max momentum, 0.23 mNm max torque

2.1 ADCS modes

Once the satellite is inserted into orbit, various control modes should be evaluated for different scenarios. These modes encompass the following: no control, only-estimation, detumbling, sun pointing, nadir pointing, and forward/backward horizon pointing.

No control: In this mode, actuators and sensors will be powered off. It is initially activated when the satellite enters orbit and in the event of critical power levels.

Only estimation: No actuation is performed in this mode, but sensor measurements are collected, and the attitude determination block estimates the attitude states.

Detumbling: This mode aims to reduce the satellite's angular rates using magnetometer measurements and magnetorquers. It is typically enabled during satellite commissioning to reduce the initial angular speed of the satellite. It can also be activated later when high angular rates are encountered.

Sun pointing: In this mode, the deployed solar panels, on the -z axis, are oriented toward the Sun. The satellite body sun vector can be determined using Sun sensors or Sun vector reference model and attitude estimates. This mode can be activated either using RW or without RW, in addition to the magnetorquers. The estimation block should provide input to the control block for this task.

Nadir pointing for communication: This mode is intended for the OPERA mission, requiring a pointing accuracy of only 40 degrees. The nadir direction vector can be obtained from the navigation block. Similar to sun pointing, nadir pointing can be enabled either using RW or without RW, along with the magnetorquers. The estimation block should provide input to the control block for this task.

Forward/backward horizon pointing: This mode represents the most demanding ADCS task for the satellite, demanding up to 8-degree pointing accuracy and requiring higher estimation accuracy to reduce errors in the light-intensity experiment analysis. The forward and backward horizon modes should be activated for observations during sunrise and sunset periods, respectively.

2.2 ADCS equipment

The equipment for the LEOPARD ADCS is listed in Table 1 and related axis definition is shown in Fig. 3. Six coarse Sun sensors, placed on each axis, are used to determine the Sun vector. Two TAM sensors, one external TAM positioned on the -z side and the other included with the magnetorquer module, provide the Earth's magnetic field vector. Two different gyroscopes have been chosen for redundancy and are used to obtain angular rates and propagate the attitude states in the attitude filter. A three-axis magnetorquer is employed for detumbling, attitude control, and momentum dumping of the RW. One RW, is used for attitude control purposes on the y-axis.

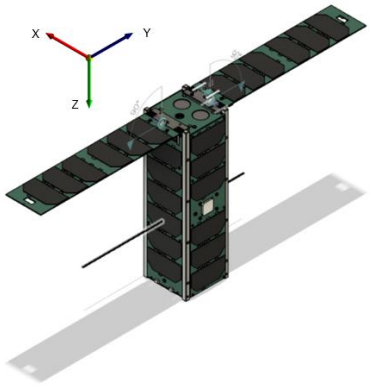

Fig. 1. LEOPARD axis definitions

2.3 Attitude determination

The attitude determination block encompasses a range of algorithms and filters aimed at precisely determining the attitude states.

Coarse attitude determination algorithm: A basic TRIAD algorithm [4] is implemented in order to process Sun vector and magnetic field vector to determine coarse attitude information. This algorithm is used to initialize EKF attitude filters and can be used to determine coarse attitude when required.

Attitude filter: The main attitude filter is EKF utilizing gyro, Sun sensor and magnetometer measurements to estimate attitude and angular rates. It employs attitude quaternion and gyro bias as Kalman states as below:

$$\boldsymbol{x} = \begin{bmatrix} \boldsymbol{q} \\ \boldsymbol{b}_{gyro} \end{bmatrix} \tag{1}$$

The gyro measurements are corrected with the gyro bias estimates, and the resulting corrected gyro measurements are directly used to propagate the attitude in the filter. TAM and Sun sensors are used in the Sun phase, whereas only-TAM is utilized in eclipse phase for the filter measurement as given below:

$$\boldsymbol{h} = \begin{cases} \begin{bmatrix} \tilde{\boldsymbol{B}}_b \\ \tilde{\boldsymbol{S}}_b \end{bmatrix} & in\ Sun\ phase \\ \tilde{\boldsymbol{B}}_b & in\ eclipse \end{cases} \tag{2}$$

In case of gyro failures, another EKF has been designed, which relies on Sun sensors and a magnetometer for attitude estimation. This filter utilizes attitude dynamics for state propagation, requiring the provision of dynamic-related parameters to the filter. Thus, the filter state vector is constructed with attitude quaternion and angular rate vectors given as:

$$\boldsymbol{x} = \begin{bmatrix} \boldsymbol{\omega} \\ \boldsymbol{b}_{gyro} \end{bmatrix} \tag{3}$$

For further details on these filters, please refer to [5].

RMM estimator: An optional RMM estimator using an EKF is designed and available onboard. This is particularly important since there may be differences between the ground-based RMM determination and what is encountered onboard [6,7]. It serves as a second stage of the attitude filter and is used for estimating the RMM as required. The filter state is represented as:

$$\boldsymbol{x} = \begin{bmatrix} \boldsymbol{\omega} \\ \boldsymbol{M}_{RMM} \end{bmatrix} \tag{4}$$

and the filter measurement equation is constructed using the estimated angular velocity from the attitude filter as given below:

$$\boldsymbol{h} = \hat{\boldsymbol{\omega}} \tag{5}$$

This filter design can estimate the RMM because the angular velocity dynamic equation includes the RMM term.

Fig. 4 illustrates the flowchart of the complete attitude determination process for LEOPARD.

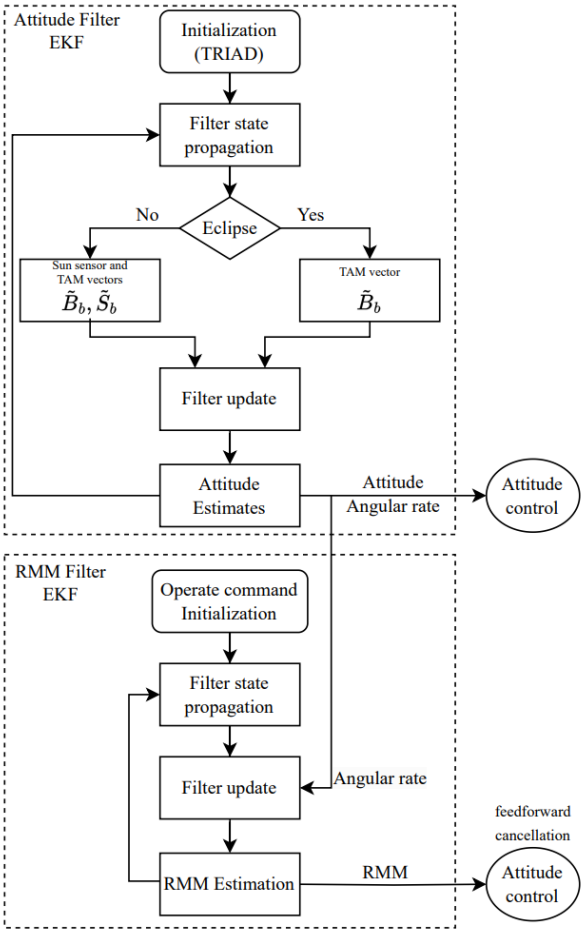

Fig. 2. Attitude determination flowchart

2.4 Attitude control

Different control algorithms are used to calculate control laws and allocate the commands to the actuators according to the operational modes.

2.4.1 Detumbling

The Bdot control algorithm, which is widely utilized for detumbling, has been implemented. In this method, the magnetorquer control moment is calculated using magnetometer readings by [8]:

$$\boldsymbol{M}_{MTQ} = -k_{Bdot} \frac{\dot{\boldsymbol{B}}_b}{\|\boldsymbol{B}_b\|^2} \tag{6}$$

where the derivative of the magnetic field can be approximated by finite difference approximation using consecutive magnetic field measurements.

2.4.2 One-axis control

Since sun pointing and nadir pointing tasks do not demand high pointing accuracy and only one-axis is required to be controlled, a one-axis control methodology is employed.

Sun pointing: The sun vector is determined through coarse Sun sensors during the sunlit period, and it is derived from the reference sun vector and attitude estimation during the eclipse phase. The desired control torque is calculated as the following:

$$\boldsymbol{T}_d = -k_c(\boldsymbol{S}_b \times \boldsymbol{S}_r) - k_\omega(\boldsymbol{\omega} - \boldsymbol{\omega}_r) \quad (7)$$

with

$$\boldsymbol{S}_r = \begin{bmatrix} 0 \\ 0 \\ -1 \end{bmatrix} \text{ and } \boldsymbol{\omega}_r = \begin{bmatrix} 0 \\ 0 \\ 0 \end{bmatrix} \quad (8)$$

Nadir pointing: The nadir vector is computed using the position vector acquired from the navigation block. The desired control torque is calculated as below:

$$\boldsymbol{T}_d = -k_c(\boldsymbol{N}_b \times \boldsymbol{N}_r) - k_\omega(\boldsymbol{\omega} - \boldsymbol{\omega}_r) \quad (9)$$

with

$$\boldsymbol{N}_r = \begin{bmatrix} -1 \\ 0 \\ 0 \end{bmatrix} \text{ and } \boldsymbol{\omega}_r = \begin{bmatrix} 0 \\ 0 \\ 0 \end{bmatrix} \quad (10)$$

2.4.3 Three-axis control for Horizon Pointing

The first step of implementing the three-axis control involves calculating a reference attitude using the following procedure: To compute the reference attitude, an interim reference attitude matrix is initially derived using position and velocity vectors obtained from the navigation block by:

$$A_{r*} = \begin{bmatrix} \bar{\boldsymbol{v}}^T \\ (\bar{\boldsymbol{r}} \times \bar{\boldsymbol{v}})^T \\ \bar{\boldsymbol{r}}^T \end{bmatrix} \quad (11)$$

This reference attitude is designed to align the satellite's z-axis with the position vector, which points in the opposite direction of the nadir vector, and to align the x-axis with the velocity vector representing the satellite's forward movement. To achieve the orientation of the -z axis toward the horizon, the interim reference attitude must be adjusted by rotating it about the y-axis at an angle of approximately ±70° in the ISS orbit. Thus, the horizon pointing reference attitude can be calculated as:

$$A_r = R_{y,\pm 70°} A_{r*} \quad (12)$$

The choice between a +70° or -70° rotation depends on whether the satellite needs to point in the backward or forward direction. After obtaining the reference attitude matrix, the reference quaternion is computed, and subsequently, the error quaternion is derived through quaternion multiplications using current and reference values. For detailed mathematical explanations related to attitude calculations, readers are encouraged to refer to [9].

The desired torque is then computed as:

$$\boldsymbol{T}_d = -k_c \boldsymbol{q}_{e,1:3} - k_\omega(\boldsymbol{\omega} - \boldsymbol{\omega}_r) \quad (13)$$

with

$$\boldsymbol{\omega}_r = \begin{bmatrix} 0 \\ 0.067 \\ 0 \end{bmatrix} \text{deg/s} \quad (14)$$

where y-axis should be aligned with the orbital angular rate for continuous pointing, and only the vector part of the quaternion is utilized in the desired torque calculation as the scalar part will be controlled implicitly due to the unit norm nature of the quaternion.

Horizon pointing in the forward direction is illustrated from the orbital plane view in Fig. 5, providing a visual representation of the required controlled attitude during sunrise.

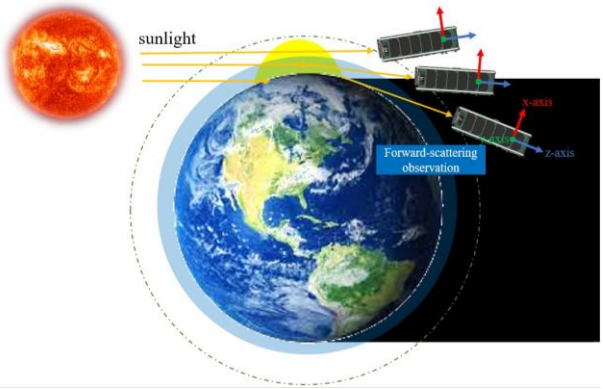

Fig. 3. Forward Horizon Pointing Illustration

2.5 Attitude control allocation

2.5.1 Control allocation for solely magnetic actuation

The sun pointing and nadir pointing algorithms yield the desired torque to be applied to the satellite. The control moment for magnetorquers is computed by projection method [10] as:

$$\boldsymbol{M}_{MTQ} = \frac{(\boldsymbol{B}_b \times \boldsymbol{T}_d)}{\|\boldsymbol{B}_b\|^2} \quad (15)$$

2.5.1 Control allocation for magnetorquers and RW

When implementing horizon pointing, all the actuators will be engaged, and occasionally, the Sun and nadir pointing scenarios may also involve the use of all actuators. Within this framework, the computed control torque is allocated to the x-axis and z-axis magnetorquers, in addition to the RW on the y-axis considering the following equation:

$$\boldsymbol{T}_d = \begin{bmatrix} 0 & 0 & -B_{b,y} \\ -B_{b,z} & 1 & B_{b,x} \\ B_{b,y} & 0 & 0 \end{bmatrix} \begin{bmatrix} M_{MTQ,x} \\ T_{rw} \\ M_{MTQ,z} \end{bmatrix} \quad (16)$$

The magnetic control moment and the RW control torque can be computed directly based on magnetic field measurements and the desired torque. This control strategy maintains controllability as long as the y-component of the magnetic field is non-zero, which occurs only momentarily.

The momentum stored in the RW is unloaded by using magnetorquers in order to prevent saturation. The magnetorquer control moment vector is computed as below:

$$\boldsymbol{M}_{MTQ} = \frac{k_d H_{rw}}{\|\boldsymbol{B}_b\|^2} \begin{bmatrix} B_{b,z} \\ 0 \\ -B_{b,x} \end{bmatrix} \quad (17)$$

where only x-axis and z-axis components of magnetorquers are utilized.

3. Simulation Results and Discussions

The algorithms for ADCS are developed and tested on MATLAB environment and this section represents the created simulation environment, ADCS equipment model, the simulation results and discussion

The satellite orbit is modelled using the ISS orbital data and orbit propagation is implemented using SGP4 [11]. The tensor of inertia of the satellite is obtained from the CAD model as

$$J = \begin{bmatrix} 6.0 \times 10^{-2} & 6.2 \times 10^{-5} & -3.1 \times 10^{-4} \\ 6.2 \times 10^{-5} & 4.7 \times 10^{-2} & -7.6 \times 10^{-4} \\ -3.1 \times 10^{-4} & -7.6 \times 10^{-4} & 2.0 \times 10^{-2} \end{bmatrix} \text{kgm}^2.$$

The zero-mean Gaussian white-noise for the Sun direction vector is taken as 0.01 which could be considered as coarse sun sensor noise. The magnetic field measurements are generated with zero-mean Gaussian white-noise, with a standard deviation of 500 nT considering the magnetic field model and the calibration errors. This assumption is made based on the use of MEMS magnetometers and these magnetometers are fully calibrated. In gyro measurement modelling, rate noise is taken as 0.0054°/s and the bias instability noise is considered as 0.00068°/s^2. For the actuator models, the specifications in Table 1 are utilized and the magnetorquers maximum duty cycle is taken as 0.7. Furthermore, for the simulations, RMM value is set to

$$\boldsymbol{M}_{RMM} = [-0.025 \quad 0.022 \quad 0.019] Am^2,$$

based on the data from previous CubeSat missions.

3.1 Detumbling Simulations

Fig. 6 illustrates the results of the detumbling algorithm. To simulate the tumbling motion of the satellite, each angular rate term is initially set to 10 deg/s.

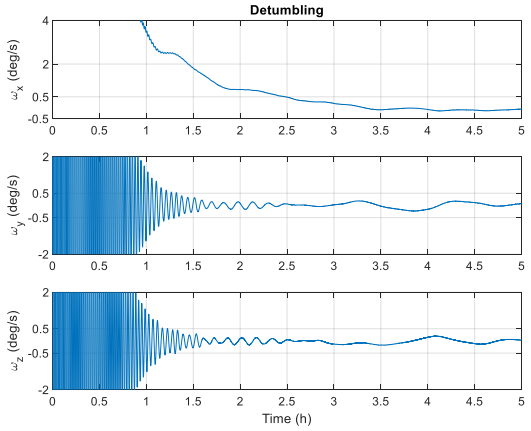

Fig. 4. Detumbling Simulation Results

After 2 orbits, which is roughly 3 hours, the angular rate values are reduced to 0.5 deg/s.

In the following algorithm simulations, the angular rates are initialized with 0.5 deg/s, as they will operate after the satellite's detumbling process.

3.2 Attitude Determination Simulations

In Fig. 7, the attitude estimation results, including roll, pitch, and yaw angles, are presented when gyro, TAM, and Sun sensor data are all utilized. The attitude filter starts estimating the attitude immediately after the eclipse period ends, and it can be observed that the attitude accuracy remains below 1 degree for each angle during the Sun phase. Furthermore, the attitude remains stable and does not experience divergence during the eclipse period, owing to the utilization of gyro and TAM sensors.

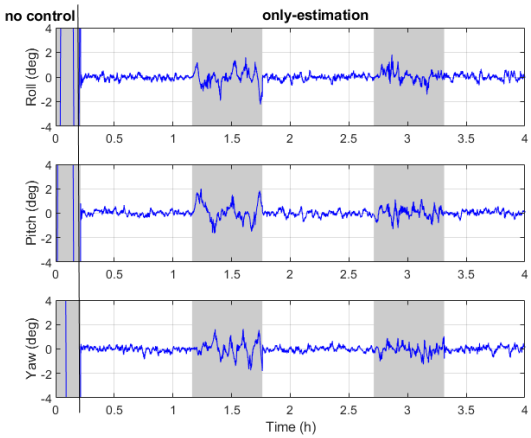

Fig. 5. Attitude estimation error by EKF using gyro, TAM and Sun sensor (shaded area: eclipse)

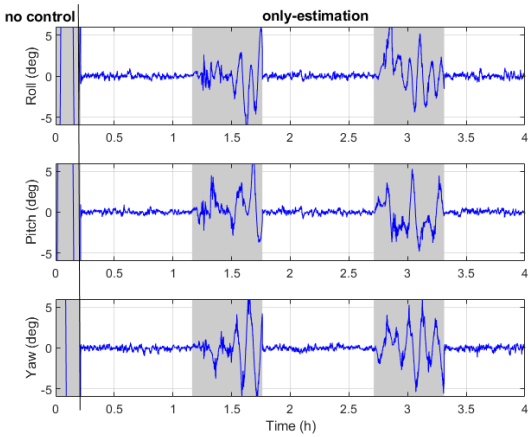

Fig. 6. Attitude estimation error by EKF using TAM and Sun sensor (shaded area: eclipse)

Regarding gyroless attitude estimation, the filter results are presented using TAM and Sun sensor in Fig. 8. The attitude angle errors remain at roughly 1 degree during the Sun phase and the attitude estimation remains stable using only-TAM measurements during the eclipse phase. However, the error is relatively higher compared to the scenario with the gyro.

The RMM estimation result is presented in Fig. 9. Initially, the attitude filter begins estimating the attitude states, and the RMM filter is activated after five minutes while waiting for the angular rate to converge. The results show the filter's ability to determine the constant RMM value, which exerts a dominant effect on the satellite.

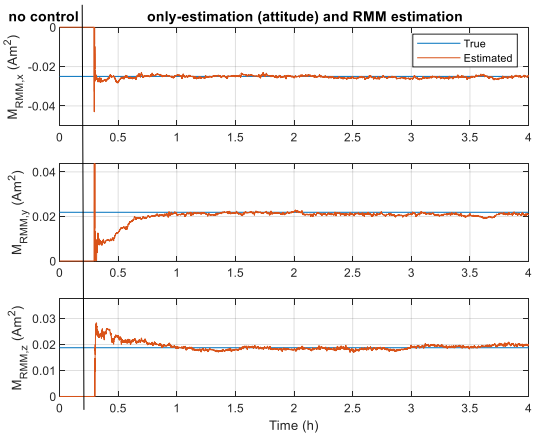

Fig. 7. RMM estimation results

3.2 Horizon Pointing

The simulations for the horizon pointing algorithms were conducted together with the Sun pointing algorithm as example scenarios. In Fig. 10, a horizon pointing scenario for Sunset horizon monitoring is presented as an example. Here, only-estimation mode is active in the first part of the simulation. Subsequently, Sun pointing algorithm is initiated, utilizing all actuators to point the satellite toward the Sun. Then, RW unloading is performed to reduce the angular momentum stored on the wheel. Finally, ADCS mode is transitioned to horizon pointing in the backward direction, enabling the satellite to perform the required pointing control for Sunset monitoring during 3–4 minutes period immediately after Sun is below the horizon rim. The result also met with the pointing requirement of the light-intensity experiment mission. Additionally, the angular momentum values of the satellite and the RW are also presented in Fig 11. It can be seen that the reaction wheel is able provide sufficient momentum and torque for this case.

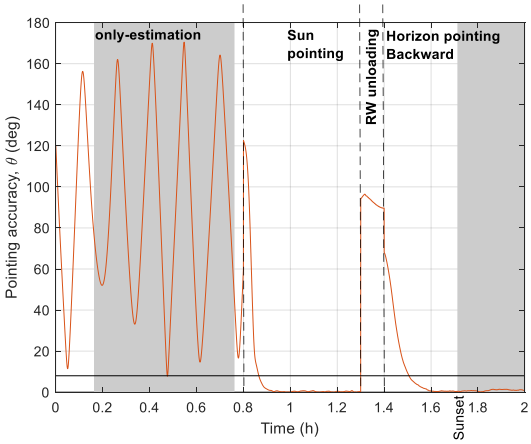

Fig. 8. Horizon pointing for Sunset horizon monitoring task

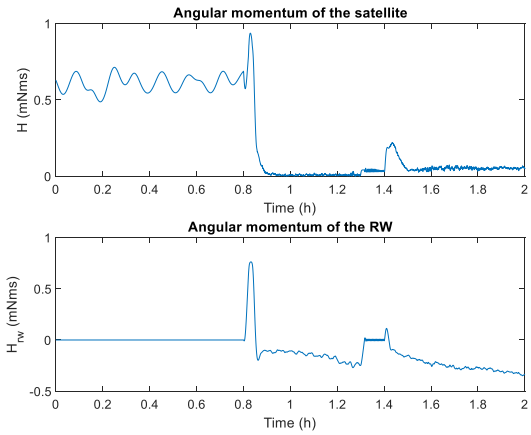

Fig. 9. Angular momentum values of the satellite and the RW for Sunset horizon monitoring

Fig. 12 illustrates the simulation results for a forward direction horizon pointing scenario. Besides, the angular momentum values of the satellite and the RW are also given in Fig 13. Similar to the previous scenario, the only-estimation mode is active initially. Then, the satellite is commanded to orient itself toward Sun. After that, RW momentum is unloaded. Finally, horizon pointing mode is initiated in the forward direction, enabling the satellite to achieve the required pointing precision for conducting Sunrise horizon monitoring effectively approximately 3-4 minutes before the Sun becomes visible above the horizon. Moreover, the RW is able to provide required performance in this case as well.

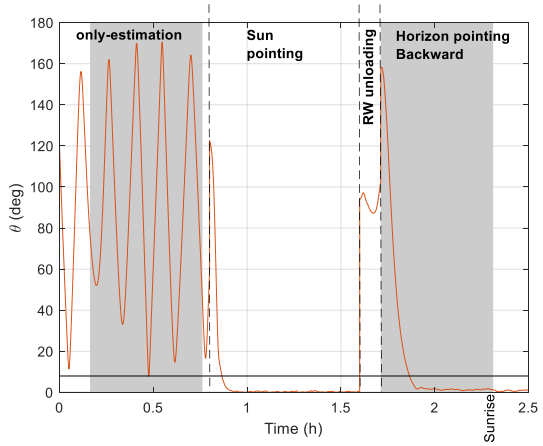

Fig. 10. Horizon pointing for Sunrise horizon monitoring task

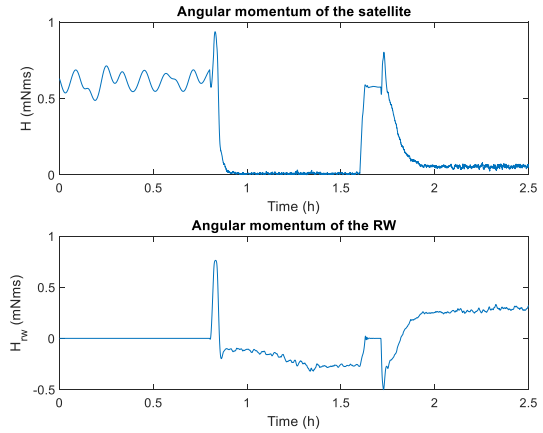

Fig. 11. Angular momentum values of the satellite and the RW for Sunrise horizon monitoring

4. Conclusions

The design of the LEOPARD ADCS, particularly its horizon pointing functionality essential for mission success, has been comprehensively detailed in this paper. The attitude determination part is designed, and the simulation results demonstrate its ability to provide attitude and angular rate information in both eclipse and Sunlit phases, ensuring a continuous feed of attitude state to the control block. Besides, a constant RMM term can be determined with the current scheme which could be used for feedforward cancellation. Sun pointing and nadir pointing algorithms are presented as well. Besides, horizon pointing algorithm has been developed and implemented, enabling the successful realization of the light-intensity experiment. Based on the simulated scenarios for horizon pointing, which encompass both forward and backward directions, and include a switching from Sun pointing to horizon pointing, it can be observed that the designed ADCS system complies with the requirement for horizon pointing. These simulation results affirm the system's capability to achieve the necessary pointing accuracy and ensure the successful execution of horizon pointing tasks in various operational scenarios.

References

[1] C. Cappelletti, S. Battistini, B. Malphrus, CubeSat Handbook: From Mission Design to Operations, Academic Press, Cambridge, MA, USA, 2020.

[2] N.C. Orger et al., Horyu-VI: International CubeSat Mission to Investigate Lunar Horizon Glow, 71st International Astronautical Congress – The CyberSpace Edition, 2020, 12–14 October.

[3] N.C. Orger, V.H. Schultz, J.R. Cordova-Alarcon, M.P. Anh, M. Cho, Multispectral Camera Payload to Monitor Orbital Sunrise and Sunset with LEOPARD 3U CubeSat – a Technology Demonstration Mission for a Lunar CubeSat, 14th IAA Symposium on Small Satellites for Earth System Observation, Berlin, Germany, 2023, 7–12 May.

[4] H.D. Black, A passive system for determining the attitude of a satellite, AIAA Journal 2 (1964) 1350-1351.

[5] M. Esit, S. Yakupoglu, H.E.Soken, Attitude filtering for nanosatellites: A comparison of different approaches under model uncertainties, Advances in Space Research 163 (2010) 51–59.

[6] S. Sakai, Y. Fukushima, H. Saito, Design and on-orbit evaluation of magnetic attitude control system for the "REIMEI" microsatellite, 10th IEEE International Workshop on Advanced Motion Control, Trento, Italy, 2008, 26–28 March.

[7] H. Ehrpais, J. Kütt, I. Sünter, E. Kulu, A. Slavinskis, M. Noorma, Nanosatellite spin-up using magnetic actuators: ESTCube-1 flight results, Acta Astronautica, 128 (2016) 210–216.

[8] G. Avanzini, F. Giulietti, Magnetic Detumbling of a Rigid Spacecraft, Journal of Guidance Control and Dynamics 35 (2012), 1326–1334.

[9] F. L. Markley, J. L. Crassidis, Fundamentals of Spacecraft Attitude Determination and Control, Springer, New York, 2014.

[10] M. Y. Ovchinnikov, D. Roldugin, A survey on active magnetic attitude control algorithms for small satellites, Progress in Aerospace Sciences 109 (2019).

[11] F.R. Hoots and R.L. Roehrich, Spacetrack Report No. 3, Models for Propagation of NORAD Element Sets, United States Air Force Aerospace Defense Command, USA, 1980.